

# XMM-Newton and Suzaku Spectroscopic Studies of Unidentified X-ray Sources towards the Galactic Bulge: 1RXS J180556.1–343818 and 1RXS J173905.2–392615

Hideyuki MORI,<sup>1,2</sup> Yoshitomo MAEDA,<sup>3</sup> Yoshihiro UEDA,<sup>4</sup>

<sup>1</sup>*CRESST and X-ray Astrophysics Laboratory, NASA Goddard Space Flight Center, Greenbelt, MD 20771, USA*

<sup>2</sup>*Department of Physics, University of Maryland, Baltimore County, 1000 Hilltop Circle, Baltimore, MD 21250, USA*

<sup>3</sup>*Department of Space Astronomy and Astrophysics, Institute of Space and Astronautical Science (ISAS), Japan Aerospace Exploration Agency (JAXA), 3-1-1, Yoshinodai, Chuo-ku, Sagami-hara, 252-5210*

<sup>4</sup>*Department of Astronomy, Graduate School of Science, Kyoto University, Sakyo-ku, Kyoto, 606-8502*  
*hideyuki.mori@nasa.gov*

(Received ; accepted )

## Abstract

With the XMM-Newton and Suzaku observations, for the first time, we acquired broad-band spectra of two unidentified X-ray sources towards the Galactic bulge: 1RXS J180556.1–343818 and 1RXS J173905.2–392615. The 1RXS J180556.1–343818 spectrum in the 0.3–7 keV band was explained by X-ray emission originated from an optically-thin thermal plasma with temperatures of 0.5 and 1.7 keV. The estimated absorption column density of  $N_{\text{H}} \sim 4 \times 10^{20} \text{ cm}^{-2}$  was significantly smaller than the Galactic HI column density towards the source. A candidate of its optical counterpart, HD 321269, was found within  $4''$ . In terms of the X-ray properties and the positional coincidence, it is quite conceivable that 1RXS J180556.1–343818 is an active G giant. We also found a dim X-ray source that was positionally consistent with 1RXS J173905.2–392615. Assuming that the X-ray spectrum can be reproduced with an absorbed optically-thin thermal plasma model with  $kT = 1.6$  keV, the X-ray flux in the 0.5–8 keV band was  $8.7 \times 10^{-14} \text{ erg s}^{-1} \text{ cm}^{-2}$ , fainter by a factor of  $\sim 7$  than that of 1RXS J173905.2–392615 during the ROSAT observation. The follow-up observations we conducted revealed that these two sources would belong to the Galactic disk, rather than the Galactic bulge.

**Key words:** X-rays: stars<sub>1</sub> — X-rays: individual (1RXS J173905.2–392615)<sub>2</sub> — X-rays: individual (1RXS J180556.1–343818)<sub>3</sub>

## 1. Introduction

A key to decipher the dynamical formation of the Galaxy is a population study in the representative Galactic components: Galactic center, disk, and the bulge. The Galactic bulge is an old ( $> 10$  Gyr) spheroidal rotator with an angular size of  $\sim 10^\circ$ , where massive stars are considered to have ended up to compact objects such as black holes or neutron stars. Since these objects produce enormous amounts of X-rays ( $L_{\text{X}} > 10^{32} \text{ erg s}^{-1}$ ) via the accretion process, hence, the luminosity function of luminous X-ray sources provides indirect information on the distribution of primordial high-mass stars in the Galactic bulge. Because of its proximity, deep investigations in some intriguing regions were devoted to revolve spatially X-ray sources down to the X-ray fluxes of several times  $10^{-14} \text{ erg s}^{-1} \text{ cm}^{-2}$  (e.g., Galactic Bulge Survey; Jonker et al. 2011), which have never been achieved in the extragalactic survey<sup>1</sup>.

However, once we focus on moderately bright X-ray sources in the Galactic bulge, which fluxes of  $\sim 10^{-12} \text{ erg s}^{-1} \text{ cm}^{-2}$  correspond to the X-ray luminosity of  $L_{\text{X}} \sim 10^{34} \text{ erg s}^{-1}$  at

8.5 kpc, the low space density of these sources requires comprehensive mapping observations with wide-field coverage and relatively long exposures. This motivates us to develop an approach to pick up the discrete X-ray sources in the Galactic bulge from the ROSAT All-Sky Survey (RASS) data. Using the X-ray color provided in the RASS Bright Source Catalogue (RBSC; Voges et al. 1999), we made a flux-limited sample of 68 sources towards the Galactic bulge; the nature of about half of these RBSC sources remains unclear. In order to improve the completeness of the Galactic bulge X-ray sources and to construct the luminosity functions of different populations in the Galactic bulge, we now proceed a campaign of X-ray follow-up observations for spectroscopic identification to the unidentified X-ray sources. A total of 21 RBSC sources has been observed so far with Suzaku (5), XMM-Newton (5), and Chandra (11). On the basis of these follow-up observations, 3 low-mass X-ray binaries (in't Zand et al. 2005, Younes et al. 2009, Mori et al. 2012), 1 RS CVn star (Mori et al. 2012), and 1 cluster of galaxies (Mori et al. 2013) were identified.

In this paper, we report the results of two unidentified X-ray sources obtained with the XMM-Newton and Suzaku observations; these two sources turned out most likely to be foreground stars. Although these sources are unlikely to be the Galactic bulge population, these stars are available for understanding the X-ray population in the Galactic disk; our result may pro-

<sup>1</sup> The X-ray flux of  $10^{-14} \text{ erg s}^{-1} \text{ cm}^{-2}$  corresponds to the X-ray luminosity of  $\sim 10^{32} \text{ erg s}^{-1}$  at a distance of 8.5 kpc, which is  $\sim 2$  orders of magnitude smaller than the sensitivity limit of the Chandra survey of the M31 bulge ( $4 \times 10^{34} \text{ erg s}^{-1}$ ; Zhang et al. 2011)

vide a clue to resolve the enhanced soft X-ray emission below 1 keV, so-called ‘‘M-band problem’’ (e.g., McCammon & Sanders 1990), or the Galactic Ridge X-ray Emission (GRXE; Koyama et al. 1986).

We describe the observation and data reduction in section 2. The analysis of the X-ray images and spectra as well as their results are given in section 3. After the discussion on the nature of the X-ray sources in section 4, we summarize our results in section 5. We note that errors represent the 90% confidence limits throughout the paper, unless otherwise mentioned.

## 2. Observation and data reduction

Both 1RXS J180556.1–343818 and 1RXS J173905.2–392615 were first discovered with the RASS. The positions of these sources in Galactic coordinates are  $(l, b) = (357^{\circ}219, -6^{\circ}589)$  for 1RXS J180556.1–343818 and  $(350^{\circ}349, -4^{\circ}373)$  for 1RXS J173905.2–392615. The source count rates in the ROSAT PSPC band of 1RXS J180556.1–343818 and 1RXS J173905.2–392615 were  $0.29 \pm 0.05$  cts  $s^{-1}$  and  $0.07 \pm 0.02$  cts  $s^{-1}$ , respectively. In order to estimate X-ray fluxes in the 0.5–10 keV band, we assumed an absorbed power-law model with photon index of  $\Gamma = 1.7$ . From the Galactic latitude ( $b$ ) and the X-ray color for each source, the absorption column density can be estimated to  $N_{\text{H}} = (1.5\text{--}7.9) \times 10^{21}$   $\text{cm}^{-2}$  for 1RXS J180556.1–343818 and  $N_{\text{H}} = (3.6\text{--}11.7) \times 10^{21}$   $\text{cm}^{-2}$  for 1RXS J173905.2–392615. Thus, the count rates for 1RXS J180556.1–341838 and 1RXS J173905.2–392615 correspond to the absorption-corrected X-ray fluxes in the 0.5–10 keV band of  $(0.9\text{--}2.7) \times 10^{-11}$  and  $(0.3\text{--}1.0) \times 10^{-11}$   $\text{erg s}^{-1} \text{cm}^{-2}$ , respectively.

In order to obtain the broad-band X-ray spectrum, we performed the observation of 1RXS J180556.1–343818 with XMM-Newton (Jansen et al. 2001) in March 2004. XMM-Newton possesses European Photon Imaging Camera (EPIC) placed on the focus of the X-ray telescopes (Aschenbach et al. 2000) with large photon collecting area. Two of the EPIC cameras consist of 7 CCD arrays manufactured with Metal Oxide Semiconductor (MOS; Turner et al. 2001). Another EPIC camera has an array of the pn-type CCD chips (pn; Strüder et al. 2001). The observation log is given in table 1. All of the EPIC cameras were operated in the full frame mode with medium filters. The exposure times during the observation were 10.0 ks for the pn camera and 11.6 ks for the MOS cameras. The Science Analysis Software (version 13.0.1) was used to reduce the data and to create scientific products. We first reprocessed the Observation Data Files, provided by the XMM-Newton Science Archive, by running `epchain` and `emchain` tasks with the latest calibration database.

To remove the background flares produced by soft protons, we selected good time intervals (GTIs) by following the instruction in the XMM data reduction guide<sup>2</sup>. We filtered out the time intervals in which the count rate of single events (`PATTERN = 0`) over the full detector field of view was larger than 0.4 cts  $s^{-1}$  in the 10–12 keV band for pn or 0.35 cts  $s^{-1}$  above 10 keV for MOS1/2. The flare-screened live times for

the pn, MOS1, and MOS2 cameras were 384 s, 2.84 ks, and 2.94 ks, respectively.

1RXS J173905.2–392615 was observed with the Suzaku satellite (Mitsuda et al. 2007) in September 2012. The X-ray CCD cameras (XIS; Koyama et al. 2007) and the corresponding X-ray telescopes (XRT; Serlemitsos et al. 2007) onboard Suzaku enable us to perform imaging spectroscopy in the 0.2–10 keV band. The XIS consists of one back-illuminated (BI) CCD and three front-illuminated (FI) ones. However, one FI CCD (XIS2) has been out of order since November 9, 2006. Furthermore, a part of the imaging area of the XIS0 has been unusable since June 23, 2009<sup>3</sup>. The XIS was operated in the normal mode without any window and timing options. During the observation, the spaced-row charge injection (Uchiyama et al. 2009) was applied. Suzaku also equips non-imaging Hard X-ray Detector (HXD; Takahashi et al. 2007, Kokubun et al. 2007), consisting of the Si-PIN photodiodes and GSO scintillators to cover the energy band of 10–600 keV. The HXD was also operated in the normal mode. The log of the Suzaku observation is also given in table 1.

We reduced the cleaned event data which were pre-processed with the processing version of 2.8.16.34. Because of high Non-X-ray Backgrounds (NXBs), time intervals during the passage of the South Atlantic Anomaly, the low-Earth orbit, and the low Day-Earth orbit were discarded in the cleaned event data. The effective exposure time was 22.1 ks for the XIS and 17.1 ks for the HXD. The reduction tool we used here was HEASOFT (version 6.13). X-ray images, light curves, and spectra were generated by running `Xselect`. We note that the HXD-PIN count rate in the 18–40 keV band was  $0.157 \pm 0.003$  cts  $s^{-1}$ . It was consistent with that of the NXB ( $0.155 \pm 0.001$  cts  $s^{-1}$ ) derived from the ‘‘tuned background’’ file, `ae407029010_hxd_pinbgd.evt.gz`, provided from the HXD team. Since significant signals were not detected from the HXD-PIN, we focused on the XIS data in the following analysis.

## 3. Analysis

### 3.1. 1RXS J180556.1–343818

Figure 1a shows the X-ray image in the 0.5–10 keV band obtained with the XMM-Newton observation. We created the MOS1, MOS2, and pn images with a pixel size of  $5'' \times 5''$  from the respective event files. These images were added together, and then smoothed with the Gaussian function of  $\sigma = 15''$ . 1RXS J180556.1–343818 was found at the center of the MOS 1/2 field of view. Some sources outside the error radius of 1RXS J180556.1–343818 were also detected, but their detailed spectral analysis is beyond the scope of this paper. The position of the brightness peak was at  $(RA, Dec)_{\text{J2000.0}} = (18^{\text{h}}05^{\text{m}}56^{\text{s}}33, -34^{\circ}38'29''.3)$ . Hence, as a source-extraction region, we selected a circle with a radius of  $1'$  centered on this position. We chose the surrounding source-free annulus as a background region. The inner and outer radii of the annulus were set to be  $1'.67$  and  $2'.5$ , respectively.

For each sensor, we made the X-ray light curves in the 0.5–10 keV band from the source and background regions. No

<sup>2</sup> [http://xmm.esac.esa.int/external/xmm\\_user\\_support/documentation/sas\\_usg/USG.pdf](http://xmm.esac.esa.int/external/xmm_user_support/documentation/sas_usg/USG.pdf)

<sup>3</sup> Suzaku memo: JX-ISAS-SUZAKU-MEMO-2010-01

Table 1. Observation log.

Target	Observatory	Obs. ID	Start / End time (UT)	Exposure (ks)*
1RXS J180556.1–343818	XMM-Newton	0206990301	2004/03/11 07:44:37 2004/03/11 10:31:53	2.8 (MOS1), 2.9 (MOS2) 0.38 (pn)
1RXS J173905.2–392615	Suzaku	407029010	2012/09/18 19:46:11 2012/09/19 08:16:22	22.1 (XIS), 17.1 (PIN)

\* Effective exposure of the screened data. The HXD-PIN exposure is dead-time corrected.

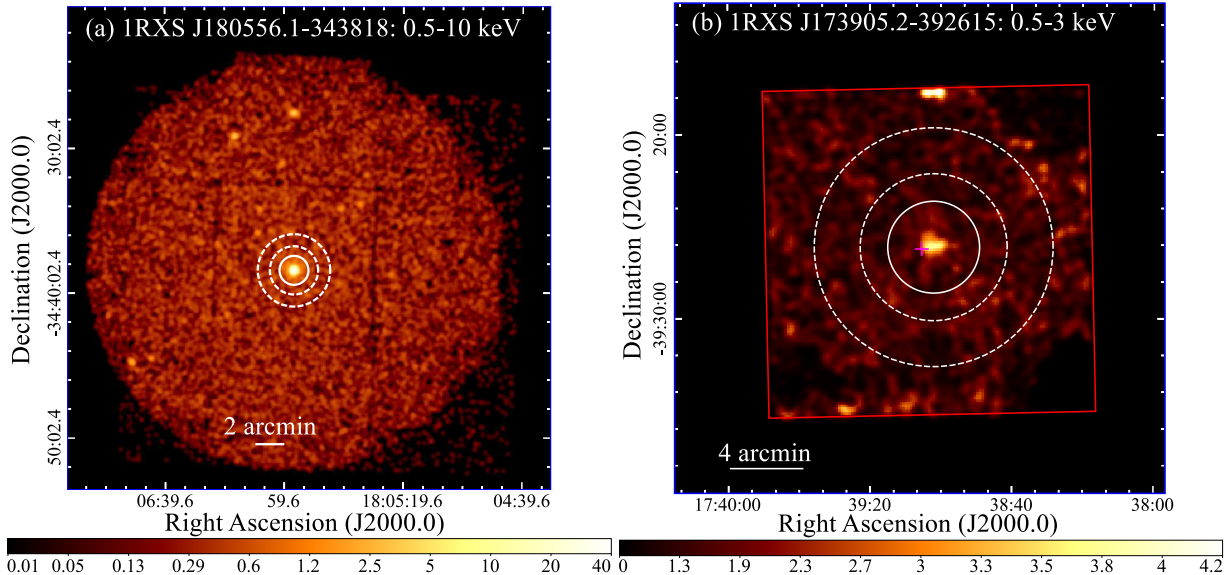


**Fig. 1.** X-ray images of 1RXS J180556.1–343818 (a, 0.5–10 keV) and 1RXS J173905.2–392615 (b, 0.5–3 keV) obtained with the XMM-Newton and Suzaku observations. The MOS1, MOS2, and pn images were binned with  $5'' \times 5''$  and then added together. The smoothing with the Gaussian function of  $\sigma = 15''$  was applied to the summed image. No vignetting correction was performed. The solid white circle and the dashed white annulus centered on 1RXS J180556.1–343818 indicate the regions to extract the source and background spectra, respectively. The XIS image was also binned with  $8 \times 8$  pixels and then smoothed with the Gaussian kernel of  $\sigma = 33''$ . The subtraction of the Non-X-ray Background and the vignetting correction were applied to the XIS image. The red square represents the XIS field of view. The source and background regions to extract the XIS spectra are indicated with the solid white circle and the dashed white annulus, respectively. The position of the RBSC source is shown with the magenta plus located in the eastern direction of the X-ray emission. The color scales at the bottom panels are in unit of photons per  $5'' \times 5''$  (a) and  $8'' \times 8''$  (b) image pixel.

significant variability was found in the background-subtracted light curve. Hence, we did not apply any additional time filters in the spectral analysis. By fitting a constant model, we estimated the average count rates for MOS1, MOS2, and pn to be  $0.11 \pm 0.01$ ,  $0.11 \pm 0.01$ , and  $0.30 \pm 0.04$  cts  $s^{-1}$ , respectively.

The X-ray spectra were extracted from the source and background regions with `evselect`. The redistribution matrix file (RMF) and ancillary response file (ARF) were created with `rmfgen` and `arfgen`, respectively. We binned these spectra so that each bin contains at least 20 photons. The background-subtracted X-ray spectra are shown in figure 2. Since the significant photons were found at  $< 7$  keV, we modelled the spectra in the 0.3–7 keV band.

First, we tried to fit the X-ray spectra with a power-law or blackbody model attenuated with the photoelectric absorption (Morrison & McCammon 1983). The abundance pattern we selected was that derived from Anders & Grevesse (1989). We multiplied the model by a constant, which is fixed at unity for the FI CCDs but is left free for the BI CCD, to absorb the uncertainty of the absolute flux calibration in each instrument. Both

simple models were unacceptable; the power-law model with  $\Gamma = 3.5$  and the blackbody model with  $kT = 0.3$  keV gave the reduced  $\chi^2$  of 2.2 and 2.7, respectively. We found a clear residual around 1 keV, indicating the presence of the  $K\alpha$  emission line from highly ionized Ne. This suggests that an optically-thin thermal plasma was responsible for the X-ray emission.

Therefore, we next tried to fit the spectra with the `apec` model that reproduces X-ray emission originated from an optically-thin thermal plasma in collisional ionization equilibrium (CIE). Although the fit was improved, it was still unacceptable in terms of the reduced  $\chi^2$  ( $103/63$  d.o.f. = 1.6). Moreover, the best-fit metal abundance of  $Z/Z_{\odot} = 0.1$  did not fully reproduce the Ne x emission line and the structure around 0.6–0.7 keV. Then, we replaced the `apec` model into the `vapec` model to determine each elemental abundance individually. Here, O, Ne, Si, S, and Fe abundances were thawed; the other abundances were fixed at 0.1 times the solar values. This model yielded an acceptable fit of  $\chi^2 = 65$  (59 d.o.f.). The best-fit parameters of the plasma temperature and the absorption column density were  $kT = 1.2$  keV and  $N_{\text{H}} = 4.0 \times 10^{20}$   $\text{cm}^{-2}$ ,



respectively. O, Ne, and S were close or overabundant to the solar values ( $Z/Z_{\odot} = 0.9\text{--}1.8$ ), whereas the Si and Fe abundances did not change significantly from  $Z/Z_{\odot} = 0.1$ .

To investigate whether the enhanced abundances of O, Ne and S were an artifact due to the single-temperature plasma model, we then added another thermal plasma component to the model. The absorption column density and the metal abundance were tied between the two plasma components. While we again allowed the elemental abundances for O, Ne, Mg, Si, and Fe to vary, the other abundances were set to  $Z/Z_{\odot} = 0.1$ . The two-temperature `vapec` model also gave an acceptable fit with  $\chi^2 = 56$  (57 d.o.f.). The best-fit model was superposed on the X-ray spectra in figure 2. Since the  $F$ -test yielded the chance probability of  $P = 1\%$  due to statistical fluctuations, this two-temperature plasma model was found to improve the fit significantly. The absorption column density of  $N_{\text{H}} = 3.3 \times 10^{20} \text{ cm}^{-2}$  was consistent with that derived from the single-temperature thermal plasma model within the error. The best-fit parameters for the plasma temperatures were  $kT = 0.5^{+0.5}_{-0.1}$  and  $1.8^{+0.5}_{-0.4}$  keV. The O, Ne, Si, S and Fe abundances relative to solar values were 1.1, 2.2, 0.3, 1.0, and 0.08, respectively. We note that, when the metal abundance except for O, Ne, Si, S, and Fe was changed to be  $Z/Z_{\odot} = 0.3$ , the best-fit parameters for  $N_{\text{H}}$ ,  $kT$ , and the elemental abundances were consistent with those derived from the case of  $Z/Z_{\odot} = 0.1$ . In the case of setting all of the abundances to be free, the trend of sub-solar Fe abundance did not change, though meaningful constraints cannot be given to the metal abundances.

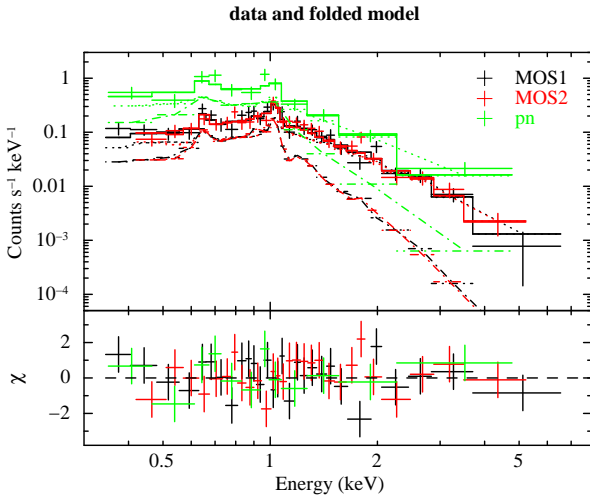


**Fig. 2.** X-ray spectra of 1RXS J180556.1–343818. The spectra obtained with MOS1, MOS2, and pn are shown with black, red, and green pluses. Solid lines overlaid on the respective spectra represent the best-fit model consisting of the two-temperature CIE plasma components. The low-temperature and high-temperature components are indicated with dash-dotted and dotted lines, respectively.

We further checked the abundances of O, Ne, and S using a multi-temperature plasma model (`cevmk1` in `XSPEC`). In this model, emission measures (EMs) are given as a function of plasma temperatures:  $dEM/dT \propto (1/T_{\text{max}})(T/T_{\text{max}})^{\alpha-1}$ . Here we can specify the maximum temperature ( $T_{\text{max}}$ ) and the power-law index ( $\alpha$ ). This multi-temperature plasma model

**Table 2.** Best-fit parameters of the 1RXS J180556.1–343818 spectra\*.

Parameters	Model <sup>†</sup>	
	<code>vapec+vapec</code>	<code>cevmk1</code>
$N_{\text{H}}$ ( $10^{20} \text{ cm}^{-2}$ )	$3.3(< 9.1)$	$4.1(< 9.6)$
$kT_1$ (keV)	$0.5^{+0.5}_{-0.1}$	—
$kT_2$ (keV)	$1.8^{+0.5}_{-0.4}$	—
$kT_{\text{max}}$ (keV)	—	$2.0^{+1.0}_{-0.6}$
$\alpha^{\ddagger}$	—	$1.8^{+1.6}_{-0.8}$
$Z_{\text{O}}^{\S}$	$1.1^{+2.1}_{-0.7}$	$0.9^{+0.9}_{-0.5}$
$Z_{\text{Ne}}^{\S}$	$2.2^{+3.6}_{-1.5}$	$1.6^{+1.6}_{-0.9}$
$Z_{\text{Si}}^{\S}$	$0.3(< 1.1)$	$0.2(< 0.8)$
$Z_{\text{S}}^{\S}$	$1.0^{+1.5}_{-0.9}$	$0.8(< 1.9)$
$Z_{\text{Fe}}^{\S}$	$0.08^{+0.21}_{-0.07}$	$0.14^{+0.21}_{-0.10}$
Normalization <sub>1</sub> <sup>l</sup>	$(4^{+15}_{-3}) \times 10^{-4}$	$(6.5^{+5.2}_{-2.8}) \times 10^{-3}$
Normalization <sub>2</sub> <sup>l</sup>	$(1.3^{+0.4}_{-0.5}) \times 10^{-3}$	—
$\chi^2/\text{d.o.f.}$	$56/57 = 0.98$	$65/58 = 1.1$
Flux (0.3–7 keV)	$1.4 \times 10^{-12} \text{ erg s}^{-1} \text{ cm}^{-2}$	

\* Superscript and subscript figures represent the upper and lower limits of the 90% confidence interval, respectively. Figures in parentheses indicate the 90% upper limit.

<sup>†</sup> Model components defined in `XSPEC`.

<sup>‡</sup> Power-law index for calculating the differential emission measure at temperature  $T$ .

<sup>§</sup> Elemental abundances relative to solar (Anders & Grevesse 1989).

<sup>l</sup> In unit of  $10^{-14}/(4\pi D^2) \int n_e n_{\text{H}} dV \text{ cm}^{-5}$ . Here  $V$  and  $D$  are the volume and distance to the plasma, respectively.

was also statistically acceptable ( $\chi^2 = 65$  (58 d.o.f.)). The best-fit maximum temperature and the power-law index were  $kT_{\text{max}} = 2.0$  keV and  $\alpha = 1.8$ , respectively. Although the elemental abundances for Si and Fe were subsolar values ( $Z/Z_{\odot} \sim 0.1$ ), the O, Ne, and S abundances were found to be 0.9, 1.6, and 0.8 times the solar values, respectively. We note that the Fe abundance was in the range of 0.02–0.34 when we re-fitted the spectra using the abundance table of Lodders (2003), instead of that of Anders & Grevesse (1989). Furthermore, the Fe abundance was estimated to be  $Z/Z_{\odot} = 0.3^{+0.7}_{-0.2}$  when all of the abundances were set to be free.

The best-fit parameters obtained with the two-temperature and multi-temperature plasma models were summarized in table 2. The X-ray flux in the 0.3–7 keV band was  $1.4 \times 10^{-12} \text{ erg s}^{-1} \text{ cm}^{-2}$ .

### 3.2. 1RXS J173905.2–392615

The XIS image of the 1RXS J173905.2–392615 field in the 0.5–3.0 keV band is shown in figure 1b. We made an XIS image with a binning of  $8 \times 8$  pixels for each sensor. After the corresponding NXB image created with `xisnxbgen` (Tawa et al. 2008) was subtracted, we divided the image by a sensitivity map at 1 keV to mitigate the XRT’s vignetting effect. The sensitivity map was produced with `xissim` (Ishisaki et al. 2007). The vignetting-corrected images were then added together. Finally, the summed image was smoothed with the Gaussian function with  $\sigma = 33''$ . X-ray emission was detected near the position of the RBSC source (magenta plus in figure 1b). The peak of the X-ray brightness was located at  $(RA, Dec)_{\text{J2000.0}} = (17^{\text{h}}39^{\text{m}}02^{\text{s}}.0, -39^{\circ}26'07'')$ .

The X-ray source, designated as Suzaku J1739–3926 here-

after, was extremely dim. Thus, we made a radial profile of the surface brightness (see figure 3) from the XIS image in the 0.5–3 keV band. Here we set the origin of the radial profile to the position of the peak brightness. We fitted the radial profile within  $7'$  with the Point Spread Function (PSF) of the XRT plus a constant model. The PSF was derived from the XIS image of SS Cyg that was used for the in-flight calibration (Serlemitsos et al. 2007). The peak of the PSF was normalized to be unity. We then set the PSF normalization and the constant to be free parameters. This model gave a marginally acceptable fit of  $\chi^2 = 29$  (20 d.o.f.). The best-fit parameters were 3.1 for the PSF normalization and 1.4 for the constant. Due to the limited photon statistics, we cannot rule out the possibility that multiple discrete sources or diffuse hot gas contribute to Suzaku J1739–3926. However, in the following analysis, we presumed that the emission comes from a single point source.

In order to determine the source position more accurately, we fitted a 2-dimensional PSF model to the vignetting-corrected image before applying the Gaussian smoothing. The PSF model was constructed from an analytical form that consists of the 3 Gaussian and 1 exponential components, which well reproduced the PSF (dashed line in figure 3) within  $4'$ . A  $2 \times 2$  binning was applied to the image to increase photon statistics per each pixel for the  $\chi^2$  minimization. We set the normalization and the center of the PSF to be free parameters. The best-fit position of Suzaku J1739–3926 was  $(RA, Dec)_{J2000.0} = (17^{\text{h}}39^{\text{m}}02^{\text{s}}.8, -39^{\circ}25'56'')$ . The PSF fit gave the 90% errors in the  $RA$  and  $Dec$  directions as  $5''$  (east),  $12''$  (west),  $4''$  (north), and  $7''$  (south). In addition, taking into account the absolute positional uncertainty for Suzaku pointing observations (Uchiyama et al. 2008), we estimated the positional accuracy of Suzaku J1739–3926 to be  $\sim 22''$ .

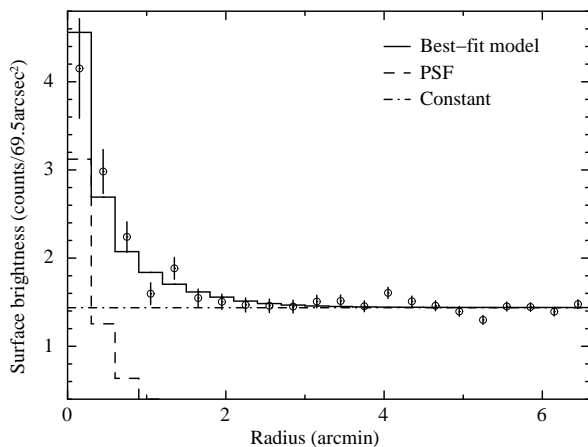


**Fig. 3.** Radial profile of the surface brightness of Suzaku J1739–3926. The vertical bars on the data represent a  $1\sigma$  statistical error. The solid line indicates the best-fit model consisting of the Point Spread Function of the XRT (dashed line) and a constant (dash-dotted line).

The source and background regions to extract the XIS spectra are shown by a solid circle and a dashed annulus in figure 1b, respectively. On the basis of the radial profile of the surface brightness, we determined the radius of the source-extraction region to be  $2.5'$ . The inner and outer radii of

the annulus for the background region were set to be  $4'$  and  $6.5'$ , respectively. The RMF and ARF were created with `xismrfgen` and `xissimarfgen` (Ishisaki et al. 2007), respectively. Suzaku J1739–3926 was too faint to obtain accurate source spectra by subtracting the background ones applied to only the area correction; the contribution of celestial X-ray backgrounds in the source-extraction region was underestimated because of the telescope vignetting. Since the source is located at low Galactic latitude of  $b = -4.373$ , the X-ray spectra are contaminated from not only the Cosmic X-ray Background (CXB) but also the GRXE. The GRXE is characteristic of intense  $K\alpha$  emission lines from highly ionized Fe ions. Thus, the underestimated background spectra would leave a false structure around 7 keV in the source spectra.

We then generated new ARFs for the source and background regions, assuming a uniform sky with a radius of  $20'$ , designated as  $A_{\text{src}}$  and  $A_{\text{bgd}}$ , respectively. The NXB spectra for the source ( $N_{\text{src}}$ ) and background ( $N_{\text{bgd}}$ ) regions were created with `xisnxbgen`. Next, for the area correction including the vignetting effect, we made background-subtracted spectra as follows; the count rate in each energy bin,  $S$ , was given by

$$S = (S_{\text{src}} - N_{\text{src}}) - \frac{A_{\text{src}}}{A_{\text{bgd}}} \times (S_{\text{bgd}} - N_{\text{bgd}}), \quad (1)$$

where  $S_{\text{src}}$ ,  $S_{\text{bgd}}$  represent the raw count rates extracted from the source and background regions, respectively. The XIS0 and XIS3 spectra were added together to improve the photon statistics. We show the background-subtracted spectra in figure 4. These spectra were binned to contain at least 10 photons per each energy bin.

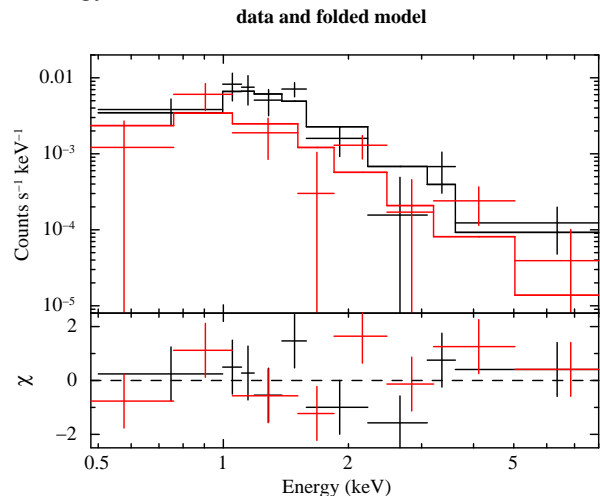


**Fig. 4.** Background-subtracted XIS spectra of Suzaku J1739–3926; FI and BI spectra are shown with black and red pluses, respectively. The solid lines represent the best-fit power-law model.

We fitted the spectrum in the 0.5–8 keV band with a power-law model (`powerlaw` in `XSPEC`) with photoelectric absorption. This model gave an acceptable fit with  $\chi^2 = 15$  (13 d.o.f.). The best-fit parameters were  $N_{\text{H}} = 1.3 \times 10^{21} \text{ cm}^{-2}$  and  $\Gamma = 3.0$ . However, because of poor photon statistics, the absorption column density cannot be constrained significantly; only the upper limit of  $N_{\text{H}} < 4.8 \times 10^{21} \text{ cm}^{-2}$  was obtained. The photon index indicated the steep soft X-ray spectra. Thus, we

**Table 3.** Best-fit parameters of the Suzaku J1739–3926 spectra\*.

Parameters	Model <sup>†</sup>	
	powerlaw	apec
$N_{\text{H}}$ ( $10^{21}$ cm <sup>-2</sup> )	1.3(< 4.8)	0(< 6.8)
$\Gamma^{\ddagger}$	$3.0^{+1.6}_{-0.7}$	—
$kT$ (keV)	—	$1.6^{+1.0}_{-0.9}$
$Z/Z_{\odot}^{\S}$	—	0.3 (fixed)
$\chi^2/\text{d.o.f.}$	15/13 = 1.2	16/13 = 1.3
Flux (0.5–8 keV)	$8.7 \times 10^{-14}$ erg s <sup>-1</sup> cm <sup>-2</sup>	

\* Superscript and subscript figures represent the upper and lower limits of the 90% confidence interval, respectively.

<sup>†</sup> Model components defined in XSPEC.

<sup>‡</sup> Photon index of the power-law continuum.

<sup>§</sup> Elemental abundances relative to solar (Anders & Grevesse 1989).

also employed a CIE plasma model (apec in XSPEC) with photoelectric absorption. The metal abundance was fixed to be  $Z/Z_{\odot} = 0.3$ . An acceptable fit was yielded again; while the best-fit temperature was found to be  $kT = 1.6^{+1.0}_{-0.9}$  keV, the upper limit of  $N_{\text{H}} < 6.8 \times 10^{21}$  cm<sup>-2</sup> was derived for the absorption column density. The best-fit parameters were summarized in table 3. In order to estimate the correct X-ray flux, we took into account a fraction of the photon flux within the source-extraction region using the XRT’s encircled energy function (Serlemitsos et al. 2007). The X-ray flux in the 0.5–8 keV band was  $8.7 \times 10^{-14}$  erg s<sup>-1</sup> cm<sup>-2</sup>.

## 4. Discussion

### 4.1. 1RXS J180556.1–343818

From the XMM-Newton observation, for the first time, we revealed the broad-band (0.3–7 keV) X-ray spectrum of the 1RXS J180556.1–343818. The X-ray spectrum was well reproduced with an absorbed optically-thin thermal plasma model with temperatures of 0.5 and 1.7 keV. Although the best-fit absorption column density depends on the model employed in the spectral fit, the 90% upper limit of  $N_{\text{H}} = 9.6 \times 10^{20}$  cm<sup>-2</sup> obtained with the multi-temperature plasma model was smaller than  $1.0 \times 10^{21}$  cm<sup>-2</sup>, a half of the total Galactic HI column density in the line of sight to the source (Dickey & Lockman 1990). This smaller absorption suggests that 1RXS J180556.1–343818 is a foreground source, not located in the Galactic bulge.

Using the SIMBAD Astronomical Database<sup>4</sup>, an optical counterpart to 1RXS J180556.1–343818 was searched. A rotationally variable star, HD 321269, was found at  $(RA, Dec)_{\text{J2000.0}} = (18^{\text{h}}05^{\text{m}}56^{\text{s}}454, -34^{\circ}38'29''.89)$  within the pointing accuracy of XMM-Newton ( $\sim 4''$ ). HD 321269 is classified as a G9III object. Høg et al. (2000) reported that the  $B$  and  $V$ -band magnitudes of this star were  $10.67 \pm 0.05$  mag and  $9.884 \pm 0.059$  mag, respectively. Assuming the absorption column density of  $N_{\text{H}} = 3.6 \times 10^{20}$  cm<sup>-2</sup> to the source, the color excess was calculated to be  $E(B - V) = 0.062$  mag, using the ratio of  $N_{\text{H}}$  to the color excess [ $N_{\text{H}}/E(B - V) = 5.8 \times 10^{21}$  atoms cm<sup>-2</sup> mag<sup>-1</sup>]. Thus, the intrinsic color index of  $B - V = 0.72$  mag was obtained. Since the absolute

$V$ -band magnitude for G giants was derived to be  $\sim 0.8$  mag (Allen 1973), we deduced the distance to the source of 640 pc. Although the assumed parameters used in the above estimation have relatively large uncertainties, the estimated distance reinforces that the source belongs to the Galactic disk.

The X-ray luminosity in the 0.3–7 keV is  $6.9 \times 10^{31} d_{640}^2$  erg s<sup>-1</sup>, where  $d_{640}$  represents the source distance in unit of 640 pc. This X-ray luminosity is comparable to that of fast rotating G giants, e.g., FK Comae (G5III, Gondoin et al. 2002) or  $\beta$  Ceti (G9.5III, Maggio et al. 1998), which luminosities were found to be  $(3-10) \times 10^{31}$  erg s<sup>-1</sup> in the 0.3–10 keV band and  $(1.5-2.7) \times 10^{30}$  erg s<sup>-1</sup> in the 0.2–4 keV band, respectively.

To elucidate plasma structures in stellar coronae, the distribution of the emission measures (EMs) given as a function of temperature ( $kT$ ) has been extensively examined with high-resolution spectroscopic studies using grating modules (e.g., Argiroffi et al. 2003, Audard et al. 2004, Scelsi et al. 2004, Telleschi et al. 2005, Huenemoerder et al. 2013). However, the X-ray spectra with moderate energy resolution for FK Comae and  $\beta$  Ceti are known to be well reproduced with a two-temperature plasma model, similar to that for 1RXS J180556.1–343818. The temperatures were 0.7 and 3.3 keV for FK Comae during its low flux phase, and 0.65 and 1.0 keV for  $\beta$  Ceti. The lower-temperature plasma with  $kT \sim 0.5$  keV of 1RXS J180556.1–343818 probably reflects a solar-type active region, which corresponds to a peak at  $\log T \sim 6.9$  of the EM distribution for G-type stars (Scelsi et al. 2005).

The temperature of the hot plasma ( $kT = 1.7$  keV) of 1RXS J180556.1–343818 was an intermediate value compared with those of  $\beta$  Ceti and FK Comae. As a possible origin of these hot components with  $kT > 1$  keV, a continuous flaring activity is suggested (e.g., Guedel 1997). It is still an open issue what are the main physical conditions that determine X-ray flaring activities of late-type giants. However, we note that such flaring activities may be somewhat related to the stellar rotation. Pallavicini et al. (1981) indeed pointed out the correlation between the X-ray luminosity and the projected rotational velocity ( $v \sin i$ ) for late-type stars. Torres et al. (2006) reported that the rotational velocity of HD 321269 was  $v \sin i = 33$  km s<sup>-1</sup>, while the rotational velocities of FK Comae and  $\beta$  Ceti were known to be  $\sim 160$  km s<sup>-1</sup> and  $\sim 3$  km s<sup>-1</sup>, respectively.

The elemental abundances of 1RXS J180556.1–343818 were found to be depleted for Fe. Regardless of the abundance tables and plasma codes<sup>5</sup> we used for the spectral fit, the Fe abundance was significantly lower than those of the other elements. While O and Ne have first ionization potentials (FIPs) higher than 10 eV, the FIP of Fe is 7.9 eV. Thus, the abundance pattern in the 1RXS J180556.1–343818 spectra may reflect differences of the FIPs. A similar abundance pattern was reported for HR 1099 (Brinkman et al. 2001), in which low-FIP elements are suppressed, compared with high-FIP ones. Diffusive processes involved with magnetic fields could operate elemental segregation in the corona that leads to such an FIP effect. In terms of the presence of a layer with an excess of high-FIP elements, Schmelz (1993) explained the Ne and S

<sup>5</sup> Because of the different approach to Fe-L lines, apec and cvmek1 implemented in XSPEC cause a slight difference in the spectra below 1 keV. See also [http://www.atomdb.org/Issues/Fe\\_Lambda\\_ATOMDB\\_SPEX.pdf](http://www.atomdb.org/Issues/Fe_Lambda_ATOMDB_SPEX.pdf)

<sup>4</sup> <http://simbad.u-strasbg.fr/simbad>



enrichment in the flaring solar plasma. Although HR 1099 is an RS CVn binary, the rotational velocity of HR1099 was obtained to be  $v \sin i = 40 \text{ km s}^{-1}$  (Vogt et al. 1999), comparable to that of HD 321269. Thus, the rotational velocity of the system may be a factor to influence the abundance pattern in the coronal plasma.

#### 4.2. 1RXS J173905.2–392615

In the Suzaku observation of 1RXS J173905.2–392615, we found faint X-ray emission, designated as Suzaku J1739–3926, in the center of the XIS field of view. Judging from the radial profile of the surface brightness, the X-ray emission probably originated from a single point source. The source position was given to be  $(RA, Dec)_{J2000.0} = (17^{\text{h}}39^{\text{m}}02^{\text{s}}.8, -39^{\circ}25'56'')$ , indicated with a red plus of figure 5. However, the exact position of the RBSC source (magenta plus in figure 5) was located  $34''$  away in the south-eastern direction from Suzaku J1739–3926. The positional accuracy of Suzaku J1739–3926 was estimated to be  $\sim 22''$ , taking into account the absolute pointing error in the Suzaku observation, as is shown by a red dashed circle in figure 5. This circular region overlapped with an error circle that represents a typical positional accuracy of the RBSC sources ( $\sim 25''$  for the 90% confidence limit, Voges et al. 1999). Hence, we concluded that Suzaku J1739–3926 was consistent with 1RXS J173905.2–392615.

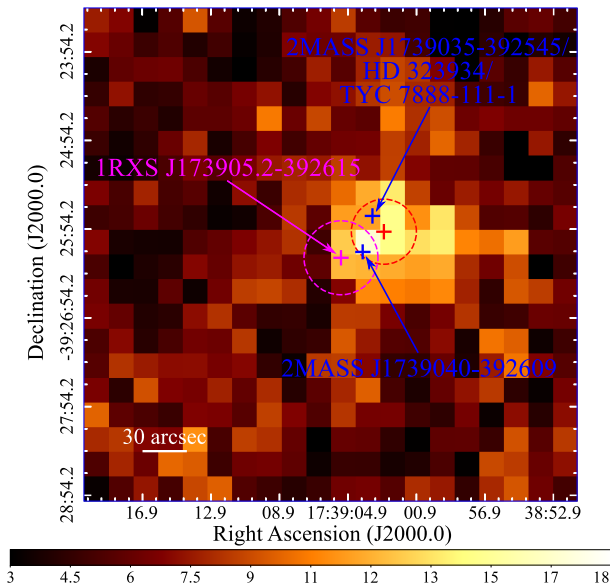


**Fig. 5.** Zoomed-up image of Suzaku J1739–3926. The vignetting correction, the binning of  $16 \times 16$  pixels, and the smoothing with  $\sigma = 16''/6$  were applied to the image. The best-fit position derived from the 2-dimensional PSF fitting is indicated with a red plus. The blue and magenta pluses represent the positions of 2MASS J1739035–392545, 2MASS J1739040–392609 and 1RXS J173905.2–392615, respectively. The positional uncertainty including the absolute accuracy of the Suzaku pointing is shown with a red dashed circle. Meanwhile, a typical positional error of the RBSC sources was drawn with a magenta dashed circle. The color scales are in unit of photons per  $16''/6 \times 16''/6$  image pixel.

We note that 10 near-infrared (NIR) sources, which are

listed in the 2MASS Second Incremental Release Point Source Catalogue (Skrutskie et al. 2006), are positionally coincident with Suzaku J1739–3926. Since no further information was available for a unique determination of the optical counterpart, hereafter, we only discuss the possibilities of the counterpart for two relatively bright (with apparent  $J$ -band magnitude of  $\lesssim 11$  mag) sources: 2MASS J1739035–392545 and 2MASS J1739040–392609.

2MASS J1739035–392545 is also identified with TYC 7888-111-1 and HD 323934 on the basis of the positional agreement. The source location of 2MASS J1739035–392545 was  $13''$  away from the best-fit position of Suzaku J1739–3926 in the north-eastern direction (blue plus in figure 5). The  $B$  and  $V$ -band magnitudes of TYC 7888-111-1 were known to be  $10.86 \pm 0.07$  mag and  $10.95 \pm 0.12$  mag, respectively, and then the spectral type of HD 323934/TYC 7888-111-1 was inferred to be A2. However, an unambiguous stellar classification is difficult; Pickles & Depagne (2010) recently derived the spectral type of F0II to HD 323934/TYC 7888-111-1 by fitting a compilation of photometric data. If 2MASS J1739035–392545/HD 323934/TYC 7888-111-1 is indeed an A-type star, we can estimate the luminosity distance as follows. Assuming the upper limit of the absorption column density to be  $N_{\text{H}} = 6.8 \times 10^{21} \text{ cm}^{-2}$ , the interstellar extinction in the  $V$ -band was estimated to be at most  $A_V \sim 3.6$  mag [ $A_V = 3.1E(B-V) = N_{\text{H}}/1.9 \times 10^{21} \text{ mag}$ ]. While the apparent  $V$ -band magnitude was  $m_V = 7.3$  mag, the absolute magnitude of A2 main sequence stars is  $M_V = 1.3$  mag. Hence, the luminosity distance was estimated to be  $\sim 160$  pc. We thus deduced the X-ray luminosity in the 0.5–8 keV band of  $2.7 \times 10^{29} \text{ erg s}^{-1}$ .

It is well known that A or F-type stars, e.g., Altair (Robrade & Schmitt 2009) and HR 8799 (Robrade & Schmitt 2010), are faint X-ray sources with  $\lesssim 10^{29} \text{ erg s}^{-1}$  and seldom show intense X-ray flares, as is explained by weak magnetic activity and stellar winds. Indeed, Altair and HR 8799 are stable in X-rays during the decades. However, assuming that the X-ray source is indeed 1RXS J173905.2–392615 and that the ROSAT spectrum is reproduced with the best-fit optically-thin thermal plasma model described in section 3.2, the source shows the flux drop from  $6.6 \times 10^{-13}$  to  $8.7 \times 10^{-14} \text{ erg s}^{-1} \text{ cm}^{-2}$ . Hence, the X-ray emission may not be attributed to 2MASS J1739035–392545. A possible scenario to explain this X-ray variability is that a hidden late-type companion of 2MASS J1739035–392545 emits soft X-rays, similar to HD 161084 (Miura et al. 2008), and that the companion was in an X-ray flaring phase during the ROSAT observation.

2MASS J1739040–392609 is located  $20''$  away from the Suzaku J1739–3926 position in the south-eastern direction (another blue plus in figure 5). The  $J$ ,  $H$ , and  $K$ -band magnitudes of the source were  $11.24 \pm 0.03$ ,  $10.61 \pm 0.02$ , and  $10.38 \pm 0.03$  mag, respectively. Since only the upper limit of the absorption column density was obtained, we should take into account a wide range of the stellar extinction ( $A_V \lesssim 3.6$  mag). Using the extinction ratios of  $A_J/A_K = 2.50$ ,  $A_H/A_K = 1.55$ , and  $A_V/A_K \sim 8.8$  (Indebetouw et al. 2005), the extinction in the respective bands were  $A_J \lesssim 1.0$ ,  $A_H \lesssim 0.64$ , and  $A_K \lesssim 0.41$  mag. Thus, the intrinsic color index of 2MASS J1739040–392609 was estimated to be  $(J-H)_0 =$

0.2–0.6 mag and  $(H - K)_0 = 0-0.2$  mag. According to table 3 of Covey et al. (2007), the combination of the color indices corresponds to main sequence stars with a spectral type of F–K. Assuming an F5V star with an absolute magnitude of  $M_J \sim 2.6$  mag (Covey et al. 2007), the luminosity distance of 2MASS J1739040–392609 is derived to be  $\sim 330$  pc, and then we can infer the X-ray luminosity of Suzaku J1739–3926 to be  $1.1 \times 10^{30}$  erg s $^{-1}$ . However, this luminosity is slightly larger than those of canonical F-type stars. We also note that the  $B$ -band magnitude of 2MASS J1739040–392609 is 15.2 mag, much fainter than that of 2MASS J1739035–392545. Thus, 2MASS J1739040–392609 may be a G or K late-type star, rather than an F-type star.

Since the information obtained from the Suzaku observation was quite limited, we cannot rule out the other possibility that Suzaku J1739–3926 is not related to 1RXS J173905.2–392615 and that the RBSC source became extremely faint below the sensitivity limit of the Suzaku XIS. The unique identification of the optical counterpart is an indispensable approach to reveal the nature of 1RXS J173905.2–392615. Therefore, the follow-up observation with Chandra would be encouraged to determine the source position more accurately, using its unprecedented high angular resolution of  $< 0''.5$ .

## 5. Summary

We conducted the XMM-Newton and Suzaku observations of the unidentified X-ray sources towards the Galactic bulge, 1RXS J180556.1–343818 and 1RXS J173905.2–392615, in order to acquire the X-ray spectrum above 2 keV. We deduced that these two sources are probably located in the Galactic disk, not in the bulge. The results of our image and spectral analysis are summarized below.

1. X-ray emission was detected at  $(RA, Dec)_{J2000.0} = (18^{\text{h}}05^{\text{m}}56^{\text{s}}.3, -34^{\circ}38'29''.3)$ , positionally coincident with a G-type giant, HD 321269, within the positional accuracy of XMM-Newton. The X-ray spectrum of 1RXS J180556.1–343818 was well reproduced with an optically-thin thermal plasma model with two temperatures affected by the photoelectric absorption. The best-fit temperatures were 0.5 and 1.7 keV. The X-ray luminosity in the 0.3–7 keV band was estimated to be  $6.9 \times 10^{31} d_{640}^2$  erg s $^{-1}$ , similar to that of rotating G giants. Compared with the O and Ne abundances, the Fe one was depleted, indicating the metal segregation. The X-ray activity and the abundance pattern in the coronal plasma should reflect the stellar rotational activity.
2. Dim X-ray emission that was positionally consistent with 1RXS J173905.2–392615 was detected. Taking into account the contribution from the Galactic Ridge X-ray Emission, we made the X-ray spectrum in the 0.5–8 keV band. Due to the limited photon statistics, the meaningful constraints to the spectral parameters were not obtained. The X-ray flux of  $8.7 \times 10^{-14}$  erg s $^{-1}$  cm $^{-2}$  was an order of magnitude fainter than that during the ROSAT observation.

We appreciate Dr. Kenji Hamaguchi and another anonymous referee for their useful and careful comments to improve our manuscript. We would like to thank all the Suzaku team members for their support of the observation and useful information on the XIS and HXD analyses. This work is also based on the observation obtained with XMM-Newton, an ESA science mission with instruments and contributions directly funded by ESA Member States and the USA (NASA). Furthermore, this publication makes use of data products from the Two Micron All Sky Survey, which is a joint project of the University of Massachusetts and the Infrared Processing and Analysis Center/California Institute of Technology, funded by the National Aeronautics and Space Administration and the National Science Foundation.

## References

- Allen, C. W. 1973, London: University of London, Athlone Press, —c1973, 3rd ed.,
- Anders, E., & Grevesse, N. 1989, *Geochim. Cosmochim. Acta*, 53, 197
- Argiroffi, C., Maggio, A., & Peres, G. 2003, *A&A*, 404, 1033
- Aschenbach, B., Briel, U. G., Haberl, F., et al. 2000, *Proc. SPIE*, 4012, 731
- Audard, M., Telleschi, A., Güdel, M., et al. 2004, *ApJ*, 617, 531
- Brinkman, A. C., Behar, E., Güdel, M., et al. 2001, *A&A*, 365, L324
- Carollo, C. M., Ferguson, H. C., & Wyse, R. F. G. 1999, *The Formation of Galactic Bulges*
- Covey, K. R., Ivezić, Ž., Schlegel, D., et al. 2007, *AJ*, 134, 2398
- Cox, A. N. 2000, *Allen's Astrophysical Quantities*,
- Dickey, J. M., & Lockman, F. J. 1990, *ARA&A*, 28, 215
- Fabricius, C., Makarov, V. V., Knude, J., & Wycoff, G. L. 2002, *A&A*, 386, 709
- García-Alvarez, D., Drake, J. J., Ball, B., Lin, L., & Kashyap, V. L. 2006, *ApJ*, 638, 1028
- Gondoin, P., Erd, C., & Lumb, D. 2002, *A&A*, 383, 919
- Güdel, M. 1997, *ApJL*, 480, L121
- Høg, E., Fabricius, C., Makarov, V. V., et al. 2000, *A&A*, 355, L27
- Huenemoerder, D. P., Phillips, K. J. H., Sylwester, J., & Sylwester, B. 2013, *ApJ*, 768, 135
- Indebetouw, R., Mathis, J. S., Babler, B. L., et al. 2005, *ApJ*, 619, 931
- Ishisaki, Y., et al. 2007, *PASJ*, 59, 113
- in't Zand, J. J. M., Cornelisse, R., & Méndez, M. 2005, *A&A*, 440, 287
- Jansen, F., Lumb, D., Altieri, B., et al. 2001, *A&A*, 365, L1
- Jonker, P. G., Bassa, C. G., Nelemans, G., et al. 2011, *ApJS*, 194, 18
- Kiraga, M. 2012, *Acta Astronomica*, 62, 67
- Kokubun, M., et al. 2007, *PASJ*, 59, 53
- Koyama, K., Makishima, K., Tanaka, Y., & Tsunemi, H. 1986, *PASJ*, 38, 121
- Koyama, K., et al. 2007, *PASJ*, 59, 23
- Lodders, K. 2003, *ApJ*, 591, 1220
- Maggio, A., Favata, F., Peres, G., & Sciortino, S. 1998, *A&A*, 330, 139
- McCammon, D., & Sanders, W. T. 1990, *ARA&A*, 28, 657
- Mitsuda, K., Bautz, M., Inoue, H., et al. 2007, *PASJ*, 59, 1
- Miura, J., Tsujimoto, M., Tsuboi, Y., et al. 2008, *PASJ*, 60, 49
- Mori, H., Maeda, Y., Ueda, Y., Dotani, T., & Ishida, M. 2012, *PASJ*, 64, 112
- Mori, H., Maeda, Y., Furuzawa, A., Haba, Y., & Ueda, Y. 2013, *PASJ*, 65, 102
- Morrison, R., & McCammon, D. 1983, *ApJ*, 270, 119
- Pallavicini, R., Golub, L., Rosner, R., et al. 1981, *ApJ*, 248, 279



- Pickles, A., & Depagne, É. 2010, *PASP*, 122, 1437
- Robrade, J., & Schmitt, J. H. M. M. 2009, *A&A*, 497, 511
- Robrade, J., & Schmitt, J. H. M. M. 2010, *A&A*, 516, A38
- Scelsi, L., Maggio, A., Peres, G., & Gondoin, P. 2004, *A&A*, 413, 643
- Scelsi, L., Maggio, A., Peres, G., & Pallavicini, R. 2005, *A&A*, 432, 671
- Schmelz, J. T. 1993, *ApJ*, 408, 373
- Serlemitsos, P. J., et al. 2007, *PASJ*, 59, 9
- Skrutskie, M. F., Cutri, R. M., Stiening, R., et al. 2006, *AJ*, 131, 1163
- Strüder, L., Briel, U., Dennerl, K., et al. 2001, *A&A*, 365, L18
- Takahashi, T., et al. 2007, *PASJ*, 59, 35
- Tawa, N., et al. 2008, *PASJ*, 60, 11
- Telleschi, A., Güdel, M., Briggs, K., et al. 2005, *ApJ*, 622, 653
- Torres, C. A. O., Quast, G. R., da Silva, L., et al. 2006, *A&A*, 460, 695
- Turner, M. J. L., Abbey, A., Arnaud, M., et al. 2001, *A&A*, 365, L27
- Uchiyama, H., et al. 2009, *PASJ*, 61, 9
- Uchiyama, Y., Maeda, Y., Ebara, M., et al. 2008, *PASJ*, 60, 35
- Voges, W., Aschenbach, B., Boller, T., et al. 1999, *A&A*, 349, 389
- Vogt, S. S., Hatzes, A. P., Misch, A. A., Kürster, M. 1999, *ApJS*, 121, 547
- Younes, G., Boirin, L., & Sabra, B. 2009, *A&A*, 502, 905
- Zhang, Z., Gilfanov, M., Voss, R., et al. 2011, *A&A*, 533, A33